Knockin mice expressing fluorescent δ-opioid receptors uncover G protein-coupled receptor dynamics *in vivo*

Grégory Scherrer*†, Petra Tryoen-Tóth*†, Dominique Filliol*, Audrey Matifas*, Delphine Laustriat*, Yu Q. Cao‡, Allan I. Basbaum§, Andrée Dierich*, Jean-Luc Vonesh*, Claire Gavériaux-Ruff*, and Brigitte L. Kieffer*¶

*Institut de Génétique et de Biologie Moléculaire et Cellulaire, Centre National de la Recherche Scientifique/Institut National de la Santé et de la Recherche Médicale/Université Louis Pasteur, 1 Rue Laurent Fries, 67404 Illkirch, France; ‡Department of Molecular and Cellular Physiology, Beckman Center, Stanford University School of Medicine, Stanford, CA 94305-5345; and §Department of Anatomy and W. M. Keck Foundation Center for Integrative Neuroscience, University of California, 513 Parnassus Avenue, San Francisco, CA 94143-2610

Communicated by Tomas Hökfelt, Karolinska Institutet, Stockholm, Sweden, May 2, 2006 (received for review October 21, 2005)

The combination of fluorescent genetically encoded proteins with mouse engineering provides a fascinating means to study dynamic biological processes in mammals. At present, green fluorescent protein (GFP) mice were mainly developed to study gene expression patterns or cell morphology and migration. Here we used enhanced GFP (EGFP) to achieve functional imaging of a G protein-coupled receptor (GPCR) *in vivo*. We created mice where the δ-opioid receptor (DOR) is replaced by an active DOR-EGFP fusion. Confocal imaging revealed detailed receptor neuroanatomy throughout the nervous system of knockin mice. Real-time imaging in primary neurons allowed dynamic visualization of drug-induced receptor trafficking. In DOR-EGFP animals, drug treatment triggered receptor endocytosis that correlated with the behavioral response. Mice with internalized receptors were insensitive to subsequent agonist administration, providing evidence that receptor sequestration limits drug efficacy *in vivo*. Direct receptor visualization in mice is a unique approach to receptor biology and drug design.

behavioral desensitization | green fluorescent protein | neuroanatomy | real-time imaging | receptor internalization

G protein-coupled receptors (GPCRs) are the largest family of membrane receptors (1) and are therapeutically essential, representing targets for 50% of marketed drugs. These receptors are highly dynamic membrane proteins that activate intracellular signaling cascades and undergo endocytosis, recycling, or degradation upon stimulation (2, 3). μ-, δ- and κ-opioid receptors are GPCRs of the nervous system, which control pain, stress, and addictive behaviors (4). δ-opioid receptors (DORs) are promising targets for the treatment of chronic pain (5) and emotional disorders (6). This opioid receptor type has fostered tremendous interest for the development of therapeutic compounds without abuse liability (7), considered a hallmark of μ-opioid agonists (8). Previously, we used the DOR as a model receptor to study mechanisms of GPCR activation (9). Here, we use this receptor as a prototype to develop GPCR imaging *in vivo*.

Fluorescent genetically encoded proteins are unique high-contrast, noninvasive molecular markers for live imaging in complex organisms. The green fluorescent protein (GFP) from the jellyfish *Aequora victoria* (10) or GFP variants (11) have become reporters of choice to study dynamic biological processes, and mouse engineering has opened the way to functional imaging in mammals (12, 13). Driven by selected promoters in transgenic mouse strains, the fluorescent reporter has revealed the localization, shape, movement, and growth of specific cell populations in neural regeneration (14) and plasticity (15) or led to building a gene expression atlas of the brain (16). In a few reports, GFP was fused to well characterized proteins by gene targeting in mice to label specific cellular compartments (14, 17).

Because the latter approach also has tremendous potential to explore the distribution and dynamics of the GFP partner, we have knocked enhanced GFP (EGFP) into the opioid δ receptor gene (*Oprd1*) and produced mice expressing a functional DOR-EGFP C-terminal fusion in place of the native DOR. These knockin mice prove to be an extraordinary tool to study receptor neuroanatomy throughout the nervous system, real-time receptor trafficking in live neurons, and receptor movements *in vivo*.

Results and Discussion

In preliminary experiments, we found that a C-terminal DOR-EGFP fusion shows unchanged binding, signaling, internalization, and down-regulation properties when expressed in HEK 293 cells (Table 1 and Movie 1, which are published as supporting information on the PNAS web site), as suggested in another study (18). We then used homologous recombination to introduce the EGFP cDNA into exon 3 of the *Oprd1* mouse gene, in frame and 5′ from the stop codon (Fig. 1 *A* and *B*). Western blot analysis of brain tissue showed expression of an EGFP-immunoreactive protein of expected size in both heterozygous and homozygous mutants (Fig. 1*C*). Quantitative mRNA analysis revealed that the genomic modification does not disrupt *Oprd1* transcription, which increased slightly in knockin animals (Fig. 1*D*). Receptor numbers (Fig. 1*E*) and maximal activations (Fig. 1*F*) increased accordingly in the DOR-EGFP mice. Affinity of the δ antagonist [^{3}H]naltrindole and potencies of selective agonists (SNC80 and deltorphin II) or the endogenous peptide Met-enkephalin were unchanged in the knockin mice (Table 2, which is published as supporting information on the PNAS web site). Therefore the endogenously expressed DOR-EGFP fully binds and responds to opioid ligands. Thus, we have successfully generated a knockin mouse expressing a fully functional EGFP-tagged δ receptor. To our knowledge, only one GFP-GPCR knockin mouse was reported. In the latter mouse, the production of a fluorescent human rhodopsin led to retinal degeneration as a consequence of a five-fold reduced receptor expression (19).

We examined the distribution of DOR-EGFP in mouse brain. Green fluorescence was detectable in the caudate putamen at birth, appeared in the hippocampus at day 3, and increased throughout the brain reaching maximal intensity at day 15 (Fig. 7, which is published as supporting information on the PNAS web site). In adult mice, strong fluorescence was observed both in whole brain and in sections (Fig. 2*A*), showing a distribution pattern concordant

Conflict of interest statement: No conflicts declared.

Abbreviations: Chat, choline acetyl transferase; DOR, δ-opioid receptor; GPCR, G protein-coupled receptor.

†G.S. and P.T.-T. contributed equally.

¶To whom correspondence should be addressed. E-mail: briki@igbmc.u-strasbg.fr.

© 2006 by The National Academy of Sciences of the USA

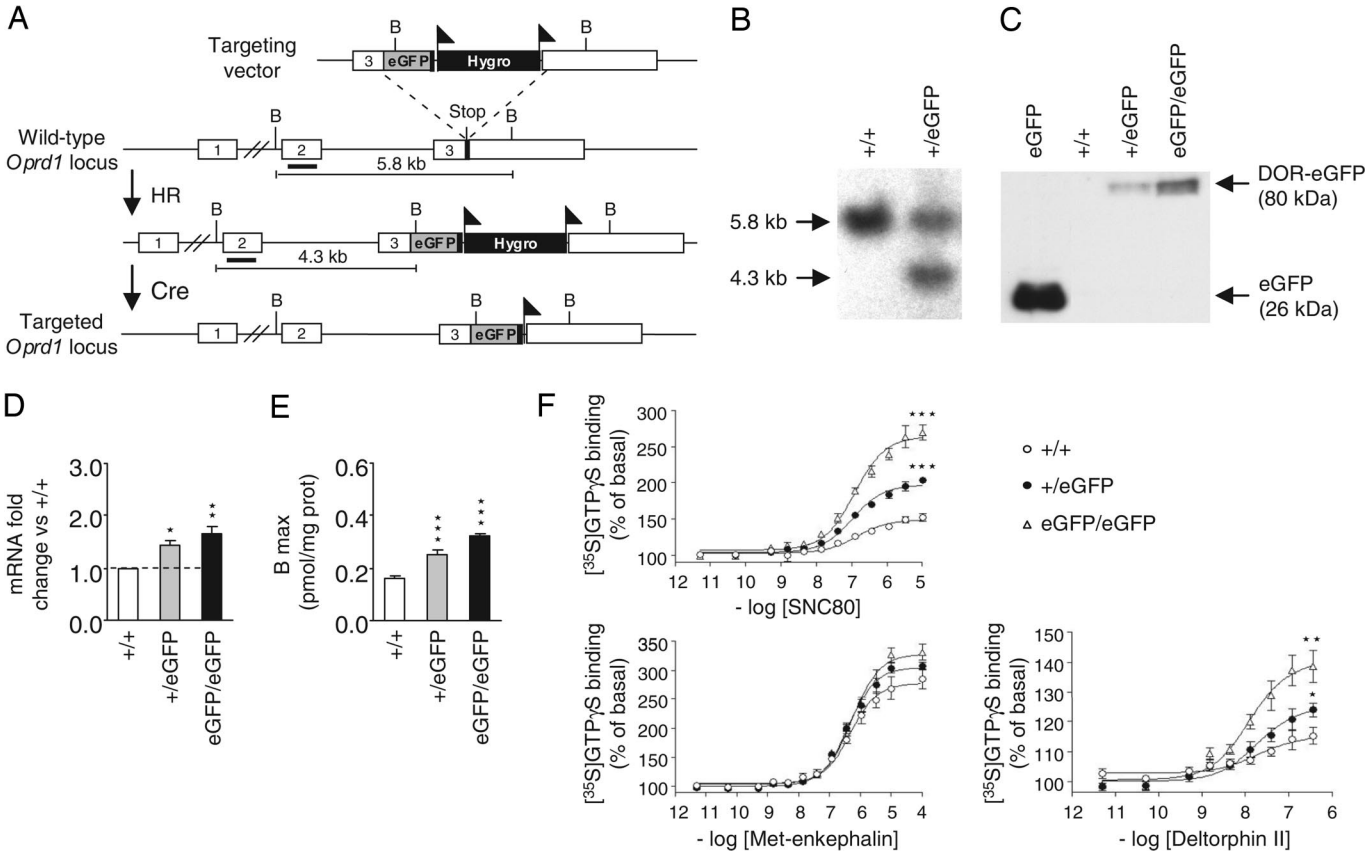

Fig. 1. DOR-EGFP knockin mice. (*A*) Targeting strategy. *Oprd1* exons, EGFP cDNA, and the floxed (triangles) hygromycine cassette are displayed as empty, gray, and black boxes, respectively. Homologous recombination (HR) was followed by Cre recombinase treatment (Cre) in ES cells. (*B*) Southern blot analysis of BamHI-digested genomic DNA from positive ES cells (right lane) by using probe shown in *A* (thick bar). (*C*) Western blot analysis of brain membrane preparations from wild-type (*Oprd1* +/+), heterozygous (*Oprd1* +/*EGFP*) and homozygous (*Oprd1 EGFP*/*EGFP*) animals by using an anti-GFP antibody, with an extract of EGFP-transfected COS cell (derived from African green monkey kidney) as a control (left lane). (*D*) Quantification of *Oprd1* transcription on RNA preparations from brains ($n = 8$). (*E*) Number of DOR binding sites in brain membrane preparations ($n = 7$). (*F*) Agonist-induced G protein activation in brain membrane preparations (SNC80, $n = 6$; Met-enkephalin, $n = 4$; deltorphin II, $n = 8$). One, two, and three asterisks correspond to *P* values for genotype effect <0.05, 0.01, and 0.001, respectively.

with previous ligand autoradiographic (20) or immunohistochemical (21) studies. Confocal imaging revealed neural structures with highly distinct architectures (Fig. 2*B*). In hippocampus and olfactory bulb, we observed numerous individual neurons with membrane fluorescence in both cell bodies and processes. In caudate putamen, fluorescent cell bodies appeared embedded in strong diffuse fluorescence, probably arising from the dense arborization of DOR-expressing neurons. Very few single cells were visible in basolateral amygdala, where intense fluorescence likely resulted from receptors on afferent fibers. We established striatal and hippocampal primary cell cultures from newborn pups (P0). In these preparations, bright fluorescence appeared in some neurons at day 3, increasing up to day 10 *in vitro*. The EGFP signal was strong at the surface of both cell bodies and processes and was also observed intracellularly mostly in the perikarya region (Fig. 2*C*).

We studied the colocalization of DOR-EGFP with GABA and choline acetyl transferase (Chat) immunoreactivities in brain areas where DOR-expressing neurons have been characterized earlier and in primary neurons (Fig. 3). Quantification of cell populations showed that most striatal cholinergic neurons expressed DOR-EGFP in brain and primary cultures, concordant with previous findings (22). We found a significant amount of GABA+/EGFP+ neurons in these samples. As predicted in ref. 23, hippocampal GABAergic neurons also showed green fluorescence. Altogether, our preliminary anatomical analysis shows that DOR-EGFP is expressed at expected neural sites and validates the DOR-EGFP mouse model to study δ receptor function both *ex vivo* and *in vivo*.

GPCR-GFP fusions are unique tools for real-time recording of receptor trafficking, as documented earlier in heterologous expression systems (24). To evaluate dynamic properties of the receptor endogenously expressed in its native environment, we exposed striatal primary neurons to three δ agonists (SNC80, deltorphin II, and Met-enkephalin; see Fig. 4 and Movies 2, 3, and 4, which are published as supporting information on the PNAS web site). All agonists triggered the clustering of receptors (bright spots) along the plasma membrane both in cell bodies and processes. DOR-EGFP clusters then progressively internalized, producing a typical vesicular punctate pattern. After 20 min, the fluorescent spots finally converged into bigger vesicles, whose nature is being examined. Whether the kinetics of receptor endocytosis is neuron-dependent or ligand-dependent, as suggested earlier in neuroblastoma cells (25), is currently under investigation. More generally, primary cultures from DOR-EGFP mice represent a potent tool to explore trafficking efficacies for a large set of opioid peptides and drugs, and determine whether internalization could serve as an index of drug efficacy *in vivo* in the process of developing novel potent compounds for the treatment of pain or anxiety. In addition, because the endogenous peptide Met-enkephalin potently internalizes DOR-EGFP receptors, the knockin mouse could serve as a reporter to detect δ receptor activation subsequent to endogenous peptide release *in vivo*. Hence, the detection of DOR endocytosis

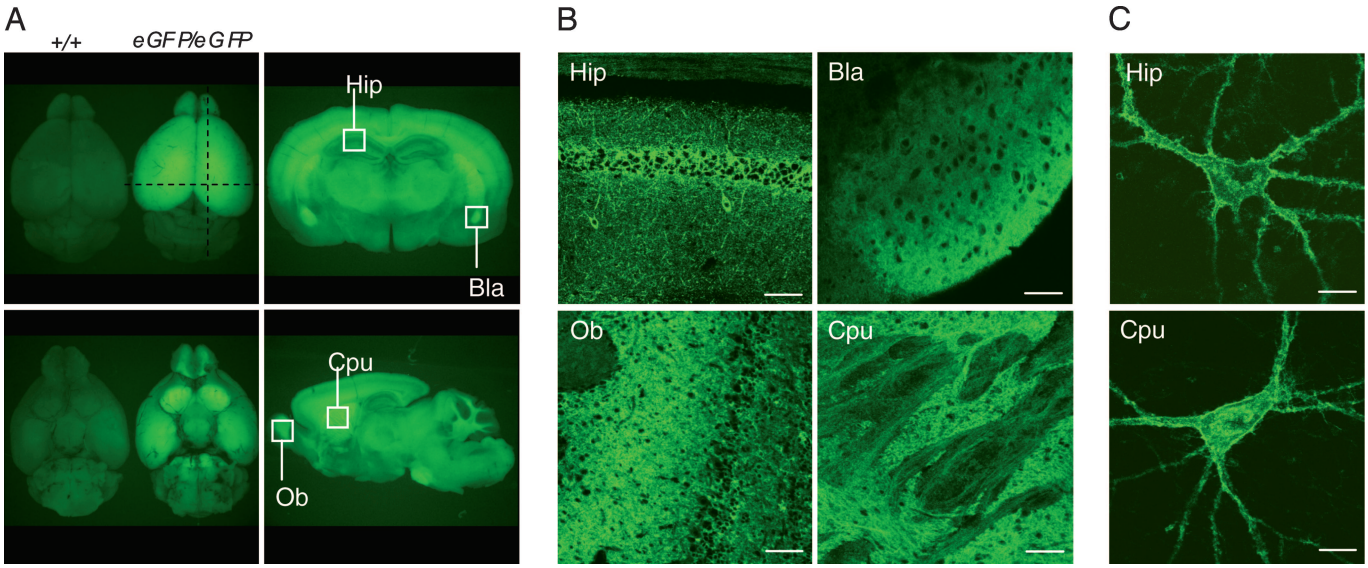

Fig. 2. Anatomical distribution of fluorescence in DOR-EGFP mice. (*A*) Macroscopic view of whole brain (*Left*), as well as coronal and sagittal brain sections of *Oprd1 EGFP/EGFP* mice (*Right*). (*B*) Confocal images of hippocampus (Hip), basolateral amygdala (Bla), olfactory bulb (Ob), and caudate putamen (Cpu), from areas indicated in *A* (*Insets*). (Scale bar: 70 μm.) (*C*) Primary neurons from Cpu and Hip. (Scale bar: 14 μm.)

under stressful or painful situations, known to recruit the endogenous opioid system, will identify sites where δ receptors operate in the nervous system.

Immunohistochemical approaches have documented GPCR endocytosis *in vivo* for μ opioid (26, 27) and substance P (28) receptors. We examined the effect of agonist treatment on the distribution of subcellular DOR-EGFP fluorescence in the knockin mice. We treated DOR-EGFP mice with either vehicle or SNC80 (10 mg/kg s.c.), known to induce δ receptor-mediated behaviors (29, 30). After 20 min, brains were removed, and receptor distribution was examined in six areas of the nervous system including central and peripheral sites (Fig. 5*A*). In the vehicle group, prominent surface fluorescence was observed in all of the neurons examined (Fig. 5*A Left*), suggesting that a significant pool of receptors is appropriately located to respond to extracellular stimuli (31). Quantification of surface versus cytoplasmic fluorescence densities (Fig. 5*B*) also showed a substantial amount of intracellular fluorescence (D_f surf/D_f cyto <2; see Fig. 5*C*). This fluorescence likely represents a receptor reserve, concordant with previous indications of intracellular DOR pools (21, 32, 33). In SNC80-treated animals, cell bodies with the typical intense punctate fluorescence were obvious throughout the nervous system (Fig. 5*A Right*), indicating that DOR-EGFPs respond to the drug by rapid endocytosis. All neurons examined so far exhibited the typical punctate pattern, and surface fluorescence generally decreased by 50% (Fig. 5*C*). *In vivo*, therefore, the drug readily recruits a pool of surface δ receptors and produces receptor sequestration throughout the nervous system.

The δ agonist SNC80 increases locomotor activity (34). To correlate receptor sequestration with a behavioral response, we

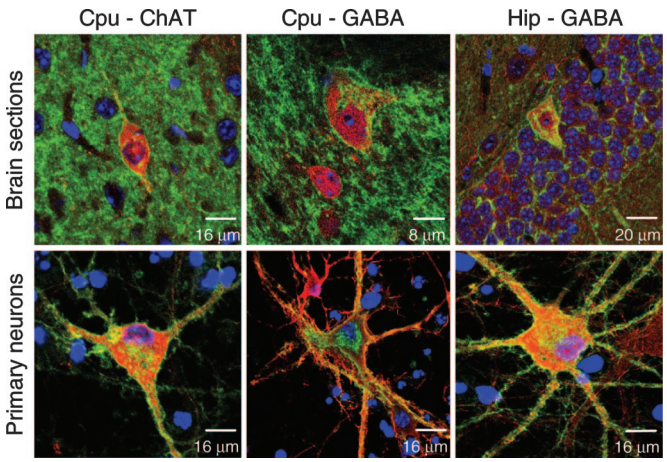

Fig. 3. Coexpression of DOR-EGFP (green) with Chat or GABA (red) in brain sections (*Upper*) and primary neurons (*Lower*) of caudate putamen (Cpu) and hippocampus (Hip). Cell nuclei are labeled with DAPI (blue). Merged, representative images are shown, and yellow indicates DOR-EGFP colocalization with either Chat or GABA. Quantification indicates that 76% of Chat+ neurons are DOR-EGFP+ in Cpu ($n = 19$) and in primary Cpu cultures ($n = 741$). Also 13% and 11% of GABA+ cells express DOR-EGFP in Cpu ($n = 31$) and Cpu cultures ($n = 2526$), respectively. In Hip and in primary Hip cultures, 13% ($n = 21$) and 25% ($n = 661$) GABAergic neurons are DOR-EGFP+, respectively.

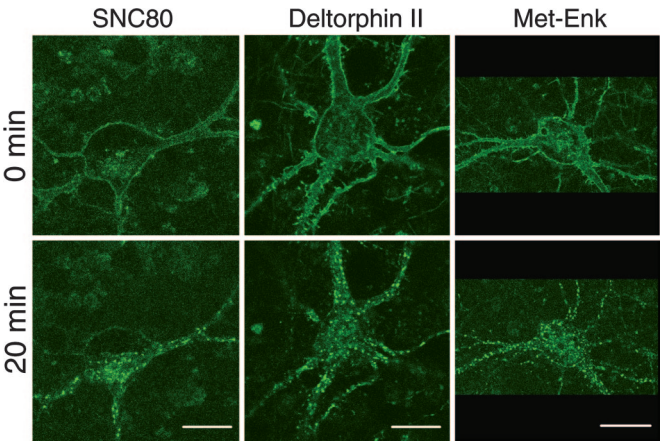

Fig. 4. Real-time confocal imaging of SNC80 (100 nM), deltorphin II (100 nM), and Met-enkephalin (1 μM)-induced DOR-EGFP redistribution in primary caudate putamen neurons (see Movies 2, 3, and 4). A representative experiment is shown ($n = 6$, 5, and 4 for SNC80, deltorphin II, and Met-enkephalin, respectively, referring to separate cell cultures from pools of 6 to 8 mouse pups). Images at 0 and 20 min of treatment, extracted from the corresponding movies, are displayed. (Scale bar: 12 μm.)

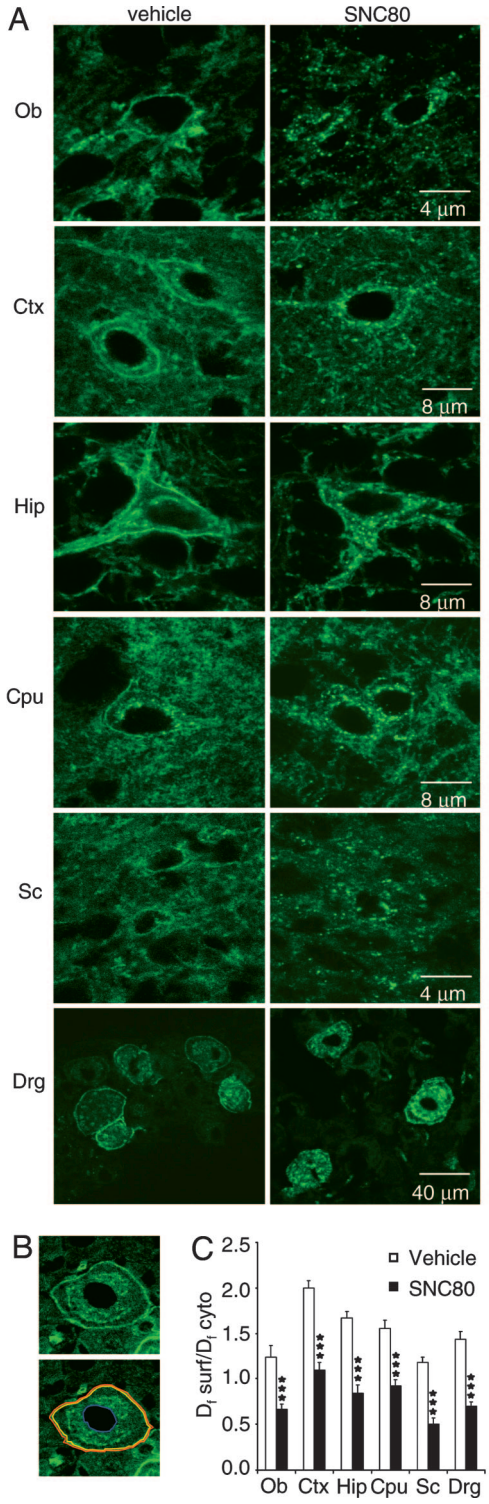

Fig. 5. DOR-EGFP endocytosis *in vivo*. (*A*) Confocal imaging of DOR-EGFP in neurons of olfactory bulb (Ob), cortex (Ctx), hippocampus (Hip), caudate putamen (Cpu), spinal cord (Sc), and dorsal root ganglia (Drg), 20 min after vehicle (*Left*) or SNC80 (10 mg/kg, s.c.) (*Right*) treatment of DOR-EGFP knockin mice. A representative image is shown from two mice per treatment (*B*) One example for quantifying subcellular fluorescence at the surface and in cytoplasmic compartments of neuron cell bodies, delimited by red/yellow and yellow/blue lines, respectively (see *Methods*). (*C*) Quantification of DOR-EGFP internalization from experiment shown in *A* and expressed as ratio of surface (D_f surf) versus cytoplasmic (D_f cyto) fluorescence densities ($n = 10$ per area per treatment). Three asterisks correspond to P value for treatment effect <0.001.

administered increasing doses of SNC80 to +/+ and EGFP/EGFP mice and measured locomotor activity. After behavioral testing (2 h), we quantified receptor endocytosis in the EGFP/EGFP mice caudate putamen, a brain region involved in this behavior. Basal locomotor activities did not differ between +/+ and EGFP/EGFP littermates (Fig. 6*A*). SNC80 produced a rapid and dose-dependent increase of locomotor activity in both wild-type and EGFP knockin animals (Fig. 6*B*). Despite the higher receptor number in EGFP/EGFP mice, this effect was comparable in the two mouse lines, suggesting the existence of a receptor reserve for the locomotor response. In δ receptor knockout mice (6), no increased locomotion was observed (Fig. 6*B*), demonstrating that this activity is mediated by δ receptors. Surface fluorescence dose-dependently decreased (Fig. 6 *C* and *D*), indicating that the endocytic response is a direct function of receptor occupancy. Interestingly, the lower dose (0.3 mg/kg) neither increased locomotor activity nor triggered any detectable endocytosis, whereas higher doses induced both. Receptor redistribution, therefore, occurs only at doses that produce behavioral activation. In fact, a noteworthy correlation exists between the number of surface receptors and locomotor activity (Fig. 6*E*). This result indicates that DOR signaling and traffic are coupled processes, likely because SNC80-receptor complexes adopt an active conformation capable to concurrently activate downstream effectors and recruit the internalization machinery. A similar observation was reported for μ-opioid receptors activated by the peptidic agonist [D-Ala^2,*N*-MePhe^4,Gly^5-ol] enkephalin (DAMGO) (26).

A currently debated issue is the functionality of surface δ receptors. Recent studies have shown that a number of stimuli induce the export of a pool of intracellular receptors to the cell surface (35–37), mostly via a regulated pathway (38), and that a functional δ response is only obtained after receptor exocytosis has occurred (39–41). Consistent with the existence of intracellular receptor pools, we show significant intracellular fluorescence throughout the nervous system of DOR-EGFP mice (Figs. 5 and 6). However, the notion that recruitment of this receptor pool is a prerequisite for functional δ responses is not supported by our behavioral data. We show that agonist exposure produces an almost immediate locomotor response, concomitant with rapid internalization of surface fluorescence. In our experimental set-up, therefore, no specific prestimulation of the system seems required to produce both receptor signaling and endocytosis *in vivo*.

In cellular systems, receptor endocytosis is proposed as one of the multiple adaptive responses leading to transient loss of receptor signaling, known as desensitization (2, 3). We studied the consequences of DOR-EGFP sequestration on receptor function *in vivo*. Groups of animals were pretreated with several SNC80 doses (Fig. 6*F*), as in the previous experiment (Fig. 6*B*). After 2 h, when DOR-EGFPs have internalized as a function of SNC80 concentration (Fig. 6*D*), we administered a second dose of 3 mg/kg to all groups (Fig. 6*F*). Animals pretreated with either vehicle or the low SNC80 dose (0.3 mg/kg), whose receptors remain on the surface, showed a significant hyperlocomotor response. On the contrary, animals pretreated with doses producing both the locomotor response and receptor redistribution (1 and 3 mg/kg) showed no significant increase of locomotor activity in response to the second injection (Fig. 6*G*). Mice with sequestered receptors, therefore, are insensitive to the agonist. This last experiment strongly suggests that DOR-EGFP sequestration prevents further DOR signaling. We propose that receptor internalization represents a main mechanism for receptor desensitization *in vivo*, a notion from many studies that has been debated by using transfected cell systems (42). Our future studies will explore the kinetics and mechanisms of receptor resensitization in the DOR-EGFP mouse. In fact, δ receptor resensitization, rather than the agonist lifetime, could be the limiting factor in the design of effective chronic drug treatments *in vivo*.

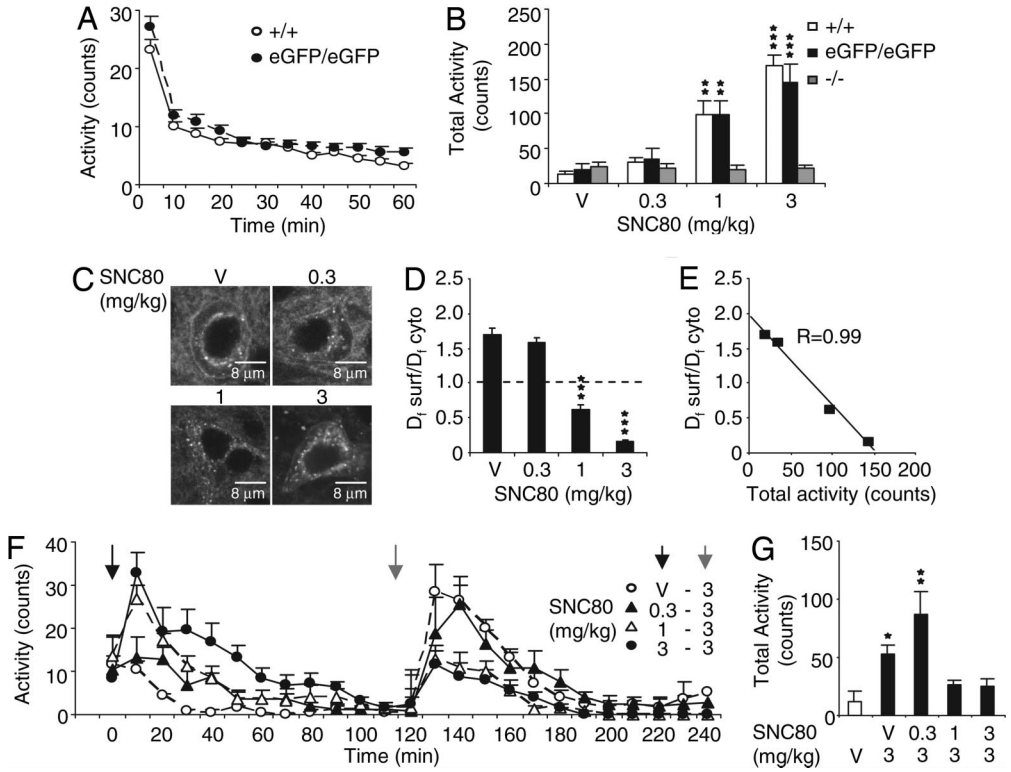

Fig. 6. DOR-EGFP endocytosis and locomotor response. (*A*) Basal locomotor activity ($n = 24$ per group). (*B*) Total locomotor activity in *Oprd1* +/+, *EGFP*/*EGFP*, and −/− mice over 2 h, after vehicle (V) or SNC80 (0.3, 1 and 3 mg/kg) administration ($n = 10$–12 per group). (*C*) Confocal imaging of DOR-EGFP in caudate putament neurons 2 h after treatments performed in *B*. (*D*) Quantification of DOR-EGFP endocytosis from experiment shown in *C* ($n = 10$ per group). (*E*) Negative correlation between surface receptors density (D_f surf/D_f cyto) and locomotor activity. (*F*) Locomotor response in *EGFP*/*EGFP* mice, in response to a first injection (black arrow) of vehicle (V) or SNC80 (0.3, 1, and 3 mg/kg) and to a second injection (gray arrow) of SNC80 (3 mg/kg) ($n = 10$ per group). (*G*) Total locomotor activity in the second 2-h period for the four experimental groups shown in *F*, compared with vehicle-treated animals (V). One, two, and three asterisks correspond to *P* values for treatment effect <0.05, 0.01, and 0.001, respectively.

Conclusion

The DOR-EGFP mouse provides a unique approach to explore receptor localization and function *in vivo*. Our first set of experiments has brought invaluable information on δ receptor neuroanatomy and biology. GPCRs represent the largest and most versatile family of membrane receptors, and each member has a specific cellular life cycle (31) and signaling regulatory mechanisms (1). The EGFP-knockin approach could be extended to other GPCRs, particularly in the case of orphan receptors for which *in vivo* pharmacology is still in its infancy.

Methods

Generation of Oprd1 EGFP/EGFP Knockin Mice. A targeting construct, where the *Oprd1* stop codon is replaced by a Gly-Ser-Ile-Ala-Thr-EGFP encoding cDNA followed by a floxed hygromycine resistance gene, was transfected into ES cells. Two independent homologous recombinants were electroporated with a Cre-expressing plasmid to excise the hygromycine gene and microinjected into C57Bl6/J blastocysts. Chimeric mice were crossed with C57Bl6/J mice to obtain F1 heterozygous progenies. Heterozygous animals were intercrossed to generate *Oprd1 EGFP/EGFP* mice that were fertile and developed normally.

Western Blotting. For Western blot analysis, 40 µg of protein from brain membrane preparations (43) were incubated at 65°C for 5 min and loaded on a 12% polyacrylamide gel. After transfer, membranes were incubated at 4°C overnight with an anti-GFP rabbit polyclonal antibody (1 µg/ml; Abcam Inc., Cambridge, MA) in blocking solution (5% milk/0.2% Tween 20/PBS). A goat horseradish peroxidase-linked anti-rabbit antibody (1:2000; Jackson ImmunoResearch) was used as a secondary antibody, and detection was performed with ECL Plus detection system (Amersham Pharmacia Biosciences).

***In Vitro* Pharmacology.** Saturation experiments were performed with [^{3}H]naltrindole (PerkinElmer) on brain membrane preparations as described (43). Agonist stimulated [^{35}S]GTPγS (PerkinElmer) binding assay was carried out with SNC80 (Tocris Cookson, Bristol, U.K), deltorphin II (Sigma), and Met-enkephalin (Sigma) on brain membrane preparations as detailed in ref. 43.

RT-PCR. Total RNA from brain was reverse-transcribed with Superscript II (Invitrogen) by using a mix of mouse *Oprd1* specific- and oligodT- primers. cDNA was used in real-time PCR experiments performed in triplicate by using iQ SYBR green supermix (Bio-Rad). Primers were 5′GCTCGTCATGTTTGGCATC and 5′AAGTACTTGGCGCTCTGGAA, encompassing exons 1 and 2 and producing a 126-bp fragment.

Primary Neurons. Newborn mice pups (P0) were decapitated, and striata and hippocampi were dissected and digested by papain (15 units/ml; Worthington) as described by Brewer (44). Cells were plated at a density of 8×10^4 cells per cm^2 on glass coverslips previously coated with polyL-lysine (PLL; Sigma), in B27/neurobasalA medium (Invitrogen) completed with 0.5 mM glutamine, 5 ng/ml basic fibroblast growth factor (bFGF, Sigma), and antibiotics. Medium was replaced without bFGF 45 min after plating, and half the medium changed after 5–7 days. Cultures were maintained until 14 days *in vitro*.

Macroscopic Imaging. Freshly dissected brains or 100-μm vibratome sections were visualized under Leica macroscope (MacroFluo; camera SpotRT). Images were acquired with IMAGEPRO software.

Confocal Microscopy. Mice were anaesthetized with a ketamine-xylazine mixture and intracardially perfused with 9.25% sucrose followed by 4% paraformaldehyde. Brain, spinal cord, and dorsal root ganglia were dissected and 50 μm vibratome or 16- to 20-μm thick cryostat sections (coexpression studies) were prepared. Primary cultures were fixed with 4% paraformaldehyde containing 4% sucrose at 10–14 days *in vitro*. Rabbit polyclonal anti-GABA (1:2,000; Sigma) and goat polyclonal anti-Chat (1:100; Chemicon) antibodies were used for immunostaining. All samples were observed under Leica confocal microscopes (SP1 or SP2UV) and the LCS (Leica) software was used for image acquisition.

Time-Lapse Confocal Microscopy. Cells were seeded in glass-bottom, 32-mm diameter plastic dishes (MatTek) coated with polyL-lysine (Sigma). Fully matured primary neurons (10–14 days *in vitro*) were used, and receptor internalization studies were performed in the presence of various drugs. Samples were observed under a Leica confocal microscope (SP2 AOBS MP) with objective 63X at 37°C. Images were automatically recorded during 20 min, with increasing time intervals to avoid bleaching effects because of repetitive scanning. Specifically, 20 frames every 10 s followed by 10 frames every 30 s, and then 12 frames every minute were recorded. Reconstituted videos (TIMT; in-house software) contain 42 images and last 2 s.

Quantification of Subcellular Fluorescence Density. Method of quantification by software IMAGEJ is shown in Fig. 5*B*. Nuclear fluorescence (within blue circle) defined the background level. Cytosolic fluorescence intensity (area between yellow and blue circles) was subtracted from whole cell fluorescence intensity (within the red circle) to obtain surface fluorescence intensity (area between red and yellow circles). Fluorescence intensity values were divided per surface unit (pixel) to obtain densities. Ratios of surface (D_f surf) versus cytoplasmic (D_f cyto) fluorescence densities was calculated to normalize data across neurons examined. A value of 1.0 results from equal densities of DOR-EGFP at the cell surface and in the cytoplasm.

Quantification of Locomotor Activity. Locomotor activity was measured by using actimetry boxes (21 cm $\times$ 11 cm $\times$ 17 cm; Imetronic, Pessac, France) contained in a soundproof cupboard. Back and forward movements were monitored via a grid of infrared beams and used as an index of locomotor activity (counts). Counts were integrated every 10 min and added to obtain total locomotor activity for a 2-h period. Animals were first habituated to actimetry cages for an hour (basal exploration). Then, measure of activity was stopped, and mice were s.c. injected with either vehicle or SNC80 (Tocris Cookson) and put back in their actimetry boxes before activity quantification was started again.

Statistical Analysis. Statistical analysis was performed with STATVIEW software by using two-way analysis of variance followed by one-way analysis of variance to study each factor separately. Differences between groups were analyzed with Bonferroni posthoc test. All results are expressed as means $\pm$ SEM.

We thank K. Befort, C. Contet, J. Becker, D. Massotte, L. Toll, and A. Vyas for critical reading of the manuscript. We thank D. Metzger (Institut de Génetique et de Biologie Moléculaire et Cellulaire) for providing the floxed hygromycine resistance cassette and A. M. Ouagazzal and H. Meziane for advice in behavioral testing. We are grateful to the transgenic and imaging core facilities of Institut de Génétique et de Biologie Moléculaire et Cellulaire. Finally, we thank P. Chambon and J. L. Mandel for their constant support. This work was supported by Centre de la Recherche National Scientifique, Institut National de la Santé et de la Recherche Médicale, University Louis Pasteur, and National Institute for Drug Abuse Grant DA05010. G.S. was a recipient of French Ministry of Research and Fédération pour la Recherche Médicale fellowships.

1. Pierce, K. L., Premont, R. T. & Lefkowitz, R. J. (2002) *Nat. Rev. Mol. Cell Biol.* **3,** 639–650.
2. Ferguson, S. S. (2001) *Pharmacol. Rev.* **53,** 1–24.
3. von Zastrow, M. (2003) *Life Sci.* **74,** 217–224.
4. Kieffer, B. L. & Gavériaux-Ruff, C. (2002) *Prog. Neurobiol.* **66,** 285–306.
5. Ahmad, S. & Dray, A. (2004) *Curr. Opin. Investig. Drugs* **5,** 67–70.
6. Filliol, D., Ghozland, S., Chluba, J., Martin, M., Matthes, H. W., Simonin, F., Befort, K., Gaveriaux-Ruff, C., Dierich, A., LeMeur, M., *et al.* (2000) *Nat. Genet.* **25,** 195–200.
7. Rapaka, R. S. & Porreca, F. (1991) *Pharm. Res.* **8,** 1–8.
8. Contet, C., Kieffer, B. L. & Befort, K. (2004) *Curr. Opin. Neurobiol.* **14,** 1–9.
9. Decaillot, F. M., Befort, K., Filliol, D., Yue, S., Walker, P. & Kieffer, B. L. (2003) *Nat. Struct. Biol.* **10,** 629–636.
10. Tsien, R. Y. (1998) *Annu. Rev. Biochem.* **67,** 509–544.
11. Feng, G., Mellor, R. H., Bernstein, M., Keller-Peck, C., Nguyen, Q. T., Wallace, M., Nerbonne, J. M., Lichtman, J. W. & Sanes, J. R. (2000) *Neuron* **28,** 41–51.
12. Ikawa, M., Yamada, S., Nakanishi, T. & Okabe, M. (1998) *FEBS Lett.* **430,** 83–87.
13. Hadjantonakis, A. K., Dickinson, M. E., Fraser, S. E. & Papaioannou, V. E. (2003) *Nat. Rev. Genet.* **4,** 613–625.
14. Nguyen, Q. T., Sanes, J. R. & Lichtman, J. W. (2002) *Nat. Neurosci.* **5,** 861–867.
15. Trachtenberg, J. T., Chen, B. E., Knott, G. W., Feng, G., Sanes, J. R., Welker, E. & Svoboda, K. (2002) *Nature* **420,** 788–794.
16. Gong, S., Zheng, C., Doughty, M. L., Losos, K., Didkovsky, N., Schambra, U. B., Nowak, N. J., Joyner, A., Leblanc, G., Hatten, M. E. & Heintz, N. (2003) *Nature* **425,** 917–925.
17. Rodriguez, I., Feinstein, P. & Mombaerts, P. (1999) *Cell* **97,** 199–208.
18. Schulz, R., Wehmeyer, A. & Schulz, K. (2002) *J. Pharmacol. Exp. Ther.* **300,** 376–384.
19. Chan, F., Bradley, A., Wensel, T. G. & Wilson, J. H. (2004) *Proc. Natl. Acad. Sci. USA* **101,** 9109–9114.
20. Goody, R. J., Oakley, S. M., Filliol, D., Kieffer, B. L. & Kitchen, I. (2002) *Brain Res.* **945,** 9–19.
21. Cahill, C. M., McClellan, K. A., Morinville, A., Hoffert, C., Hubatsch, D., O'Donnell, D. & Beaudet, A. (2001) *J. Comp. Neurol.* **440,** 65–84.
22. Lemoine, C., Kieffer, B., Gaveriauxruff, C., Befort, K. & Bloch, B. (1994) *Neuroscience* **62,** 635–640.
23. Stumm, R. K., Zhou, C., Schulz, S. & Hollt, V. (2004) *J. Comp. Neurol.* **469,** 107–118.
24. Kallal, L. & Benovic, J. L. (2000) *Trends Pharmacol. Sci.* **21,** 175–180.
25. Marie, N., Lecoq, I., Jauzac, P. & Allouche, S. (2003) *J. Biol. Chem.* **278,** 22795–22804.
26. Trafton, J. A., Abbadie, C., Marek, K. & Basbaum, A. I. (2000) *J. Neurosci.* **20,** 8578–8584.
27. Haberstock-Debic, H., Wein, M., Barrot, M., Colago, E. E., Rahman, Z., Neve, R. L., Pickel, V. M., Nestler, E. J., von Zastrow, M. & Svingos, A. L. (2003) *J. Neurosci.* **23,** 4324–4332.
28. Honor, P., Menning, P. M., Rogers, S. D., Nichols, M. L., Basbaum, A. I., Besson, J. M. & Mantyh, P. W. (1999) *J. Neurosci.* **19,** 7670–7678.
29. Broom, D. C., Jutkiewicz, E. M., Folk, J. E., Traynor, J. R., Rice, K. C. & Woods, J. H. (2002) *Neuropsychopharmacology* **26,** 744–755.
30. Saitoh, A., Kimura, Y., Suzuki, T., Kawai, K., Nagase, H. & Kamei, J. (2004) *J. Pharmacol. Sci.* **95,** 374–380.
31. Tan, C. M., Brady, A. E., Nickols, H. H., Wang, Q. & Limbird, L. E. (2004) *Annu. Rev. Pharmacol. Toxicol.* **44,** 559–609.
32. Arvidsson, U., Dado, R. J., Riedl, M., Lee, J. H., Law, P. Y., Loh, H. H., Elde, R. & Wessendorf, M. W. (1995) *J. Neurosci.* **15,** 1215–1235.
33. Wang, H. & Pickel, V. M. (2001) *J. Neurosci.* **21,** 3242–3250.
34. Broom, D. C., Nitsche, J., Pintar, J. E., Woods, J. H. & Traynor, J. R. (2002) *J. Pharmacol. Exp. Ther.* **303,** 723–729.
35. Bao, L., Jin, S. X., Zhang, C., Wang, L. H., Xu, Z. Z., Zhang, F. X., Wang, L. C., Ning, F. S., Cai, H. J., Guan, J. S., *et al.* (2003) *Neuron* **37,** 121–133.
36. Cahill, C. M., Morinville, A., O'Donnell, D. & Beaudet, A. (2003) *Pain* **101,** 199–208.
37. Commons, K. G. (2003) *J. Comp. Neurol.* **464,** 197–207.
38. Guan, J. S., Xu, Z. Z., Gao, H., He, S. Q., Ma, G. Q., Sun, T., Wang, L. H., Zhang, Z. N., Lena, I., Kitchen, I., *et al.* (2005) *Cell* **122,** 619–631.
39. Cahill, C. M., Morinville, A., Lee, M. C., Vincent, J. P., Collier, B. & Beaudet, A. (2001) *J. Neurosci.* **21,** 7598–7607.
40. Hack, S. P., Bagley, E. E., Chieng, B. C. & Christie, M. J. (2005) *J. Neurosci.* **25,** 3192–3198.
41. Walwyn, W., Maidment, N. T., Sanders, M., Evans, C. J., Kieffer, B. L. & Hales, T. G. (2005) *Mol. Pharmacol.* **68,** 1688–1698.
42. Law, P. (2004) in *The Delta Receptor*, eds. Chang, K., Porrecca, F. & Woods, J. (Dekker, New York), pp. 61–87.
43. Scherrer, G., Befort, K., Contet, C., Becker, J., Matifas, A. & Kieffer, B. L. (2004) *Eur. J. Neurosci.* **19,** 2239–2248.
44. Brewer, G. J. (1997) *J. Neurosci. Methods* **71,** 143–155.